Soft Matter

RSC Publishing

PAPER

View Article Online
View Journal

Cite this: DOI: 10.1039/c3sm50553g

Cholesterol modulates the fusogenic activity of a membranotropic domain of the FIV glycoprotein gp36†

Giuseppe Vitiello,[ab] Giovanna Fragneto,[c] Ariel Alcides Petruk,[d] Annarita Falanga,[e] Stefania Galdiero,[e] Anna Maria D'Ursi,[f] Antonello Merlino[ag] and Gerardino D'Errico*[ab]

Lipid composition of viral envelopes is usually rich in sphingolipids and cholesterol (CHOL). These components have a stiffening effect on the membrane, thus enhancing the energetic barrier to be overcome for its fusion with the T-cell plasma membrane, a fundamental step of the infection process. In this work, we demonstrate that the octapeptide (C8) corresponding to the Trp^{770}–Ile^{777} sequence of the Feline Immunodeficiency Virus gp36 is highly effective in inducing the fusion of palmitoyl oleoyl phosphatidylcholine (POPC)/sphingomyelin (SM)/CHOL membranes. We analyze the molecular mechanism of the C8–membrane interactions combining Neutron Reflectivity (NR) and Electron Spin Resonance (ESR) experiments, and molecular dynamics simulations. A strict interplay among the different lipids in the peptide-induced fusion mechanism is highlighted. Since CHOL preferentially locates close to SM, POPC molecules remain relatively free to interact with the peptide, driving its positioning at the membrane interface. Here, C8 comes in contact with CHOL-interacting SM molecules, causing a strong perturbation of acyl chain ordering, which is a necessary condition for membrane fusion. Our findings suggest that CHOL rules, by an indirect mechanism, the activity of viral fusion glycoproteins.

Received 22nd February 2013
Accepted 9th May 2013

DOI: 10.1039/c3sm50553g

www.rsc.org/softmatter

1 Introduction

For a long time, lipid bilayers were considered "inert scaffolds" with the only function of a physical barrier between the external and internal environments, whereas the membrane proteins were considered to be responsible for more specific membrane functions such as selective molecular transport, signal reception and transduction, and membrane–membrane interactions. Many recent studies have changed this concept, revealing that lipids participate actively in a variety of membrane processes.[1] Lipids can act by a "collective mechanism", in which a fine tuning of the bilayer composition regulates the physicochemical properties of the membrane, such as elasticity, curvature, surface charge and/or hydration. In particular, cholesterol and sphingolipids, carrying saturated or monounsaturated acyl chains, tend to laterally segregate from phospholipids, forming ordered domains, named "lipid rafts".[2] These domains present reduced fluidity and permeability, and preferentially incorporate some proteins, whereas (to a variable extent) they exclude others. The occurrence of lipid rafts in the membrane influences a wealth of physiological and pathological processes, *e.g.* the ion channel function, neurodegenerative processes or the regulation of T-cell signaling.[3,4]

Alternatively, single lipids can play specific roles, depending on chemical structure, conformation and dynamics of lipid headgroups and acyl chains.[5] This has promoted a wide interest in the rich biodiversity of lipids present in the various biomembranes. In particular, specific lipid molecules can be involved in signal transduction,[6] protein folding[7] or in inducing conformation and binding properties of cytolytic and antimicrobial peptides.[8] For example, it has been demonstrated that gangliosides exhibit a high affinity for neurotransmitters, influencing the receptor conformation and function, and regulate neurodegenerative mechanisms.[9] At the same inositol lipids have emerged as universal lipid regulators of protein signalling complexes in defined membrane compartments.[10] Finally, much evidence has suggested that cholesterol itself directly modulates different processes, *e.g.* the nicotinic acetylcholine receptor (nAChR) function,[11] β-amyloid fibrillization.[12,13] All these results

[a]*Department of Chemical Sciences, University of Naples "Federico II", Naples, Italy. E-mail: gerardino.derrico@unina.it*

[b]*CSGI (Consorzio per lo Sviluppo dei Sistemi a Grande Interfase), Florence, Italy*

[c]*Institut Laue-Langevin, Grenoble, France*

[d]*Departamento de Química Inorgánica, Analítica y Química Física/INQUIMAE-CONICET, University of Buenos Aires, Buenos Aires, Argentina*

[e]*Department of Pharmacy, DFM, and Centro Interuniversitario di Ricerca sui Peptidi Bioattivi, University of Naples "Federico II", Naples, Italy*

[f]*Department of Pharmaceutical Science, University of Salerno, Fisciano, Italy*

[g]*Istituto di Biostrutture e Bioimmagini, CNR, Naples, Italy*

† Electronic supplementary information (ESI) available. See DOI: 10.1039/c3sm50553g

clearly point to a decisive involvement of lipids in determining the biomembrane functionality.

Among the biological processes in which lipid membranes are involved, viral fusion is one of the most relevant. Enveloped viruses (*e.g.*, influenza virus, hepatitis C virus, human immunodeficiency virus, herpes virus) possess a lipid membrane, referred to as the envelope, usually rich in sphingolipids and cholesterol.[14] In these cases, viral infection requires a sequence of fusion and fission events between the envelope and the target membranes for entry into the cell. These energetically unfavorable processes are facilitated by the action of specific viral membrane glycoproteins.[15] It is thought that different domains of these proteins cooperate, according to a concerted mechanism of action, in driving membrane fusion. In particular, the membrane-proximal external region (MPER), also named pre-transmembrane domain,[16] has been demonstrated to be fundamental in lowering the energy barrier thus allowing the final fusion of the membranes. In this scientific framework, we have recently focused our interest on a octapeptide, named C8, corresponding to the Trp^{770}–Ile^{777} sequence of the MPER domain of the Feline Immunodeficiency Virus (FIV) glycoprotein gp36. Our studies demonstrated that C8 exerted a destabilizing effect on bilayers, perturbing the lipid packing and mobility.[17,18]

While the role played by the viral glycoproteins in the membrane fusion process is well established at a mechanistic level, the role of the lipid counterpart has not been definitely clarified. Indeed, some studies report that cholesterol and sphingolipids play key roles in the membrane-internalization of the hepatitis C virus, and that portions of structural proteins are localized at lipid-raft-like membrane structures within cells.[19] At the same time, other evidence has indicated that, for fusion between influenza virus and liposomes, the inclusion of cholesterol and sphingolipids has marked effects on pore formation.[20] However, it has not been defined yet whether cholesterol and/or sphingomyelin favor the viral infection by regulating membrane biophysical properties or by specific lipid–glycoprotein interactions.

In this scenario, the present work aims at investigating the mechanism through which the lipid composition regulates the interaction of the C8 peptide with lipid bilayers. First, we present lipid mixing assays in order to correlate the peptide fusogenic activity with lipid composition of the bilayer. Second, the interaction of the peptide with lipid bilayers, in the absence and presence of cholesterol and sphingomyelin, is investigated by Neutron Reflectivity (NR) and Electron Spin Resonance (ESR) experiments. Finally, experimental investigations are combined with molecular dynamics (MD) simulations to obtain a description of structural and dynamic behaviour of the system at the molecular level.

2 Materials and methods

2.1 Materials

The molecular formulae of some substances used in this study are presented in Fig. 1. The phospholipid palmitoyl oleoyl phosphatidylcholine (POPC) was purchased from Avanti Polar Lipids (Birmingham, AL, USA). POPC was chosen because it includes both a saturated (C16) and an unsaturated (C18) fatty acid, like most phospholipids present in mammalian cell membranes.[21] The fluorescent probes *N*-(7-nitro-benz-2-oxa-1,3-diazol-4-yl) phosphatidylethanolamine (NBD-PE) and *N*-(lissamine-rhodamine-B-sulfonyl) phosphatidylethanolamine (Rho-PE) were also purchased from Avanti Polar Lipids, while cholesterol (CHOL), sphingomyelin (SM) and Triton-X100 were obtained from Sigma (St. Louis, MO, USA). The fluorophore 8-aminonaphthalene-1,2,3-trisulfonic acid (ANTS) and the quencher *p*-xylylenebis(pyridinium bromide) (DPX), used in vesicle leakage assays, were purchased from Molecular Probes, Inc. (Junction City, OR, USA).

Spin-labeled phosphatidylcholines (*n*-PCSL) with the nitroxide group at different positions, *n*, in the *sn*-2 acyl chain, to be used for ESR experiments, were synthesized as described by Marsh and Watts.[22,23] Sphingomyelin spin labeled at the 5-th positions in the *N*-acyl chain was synthesized as described by Collado *et al.*[24] The spin-labels were stored at −20 °C in ethanol solutions at a concentration of 1 mg mL^{-1}. Ultrahigh-quality water (Ω = 18.2 Mohmcm; Elga) was used in all experiments. D_2O (99% purity) for NR experiments was provided from the Institut Laue-Langevin (ILL) in Grenoble, France.

2.2 Peptide synthesis

The amino acid sequence of the C8 peptide is Ac-Trp-Glu-Asp-Trp-Val-Gly-Trp-Ile-CO-NH_2 and the deuterated C8-d_{5all} was synthesized including Trp-d_5 in all the Trp positions. Trp-d_5 including deuteron atoms on indole ring and NH-Fmoc protected group (L-tryptophan-N-Fmoc(indole-D5), 98%) was purchased from Cambridge Isotope Laboratories Inc. (Andover, MA, USA). C8 and C8-d_{5all} were synthesized on a manual batch synthesizer (PLS 4°-4, Advanced ChemTech, Louisville, KY, USA) using a Teflon reactor (10 mL), applying the Fmoc/^{t}Bu solid phase peptide synthesis (SPPS) procedure as previously described.[18] Purified peptides (purity higher than 98%) were obtained with good yields (30–40%).

2.3 Liposome preparation

In all measurements, bilayers with two different compositions were alternatively tested: POPC alone and POPC/SM/CHOL mixtures (1 : 1 : 1 wt/wt/wt). POPC forms bilayers in the liquid-disordered state (L_α). The POPC/SM/CHOL lipid mixtures form bilayers with a rich phase behavior. Depending on the composition, the L_α, liquid-ordered L_o and/or a gel state (L_β) can occur and eventually coexist.[25] At the composition used in this work, the entire bilayer is in the L_o state.[26] Indeed, this has been one of the criteria for the choice of the composition to be used: in the case of phase coexistence, averaged (for fluorescence and NR studies) or superimposed data (for ESR measurements) would have been obtained, hampering a reliable interpretation of the results. For NR and ESR measurements, bilayers formed by POPC/CHOL mixtures (90 : 10, 80 : 20, 66 : 33 wt/wt) were also considered. On increasing the CHOL content, bilayers pass from a L_α to a L_o state.[27] Particularly, samples containing 33% w/w of CHOL present only one-phase L_o bilayers.[26,28]

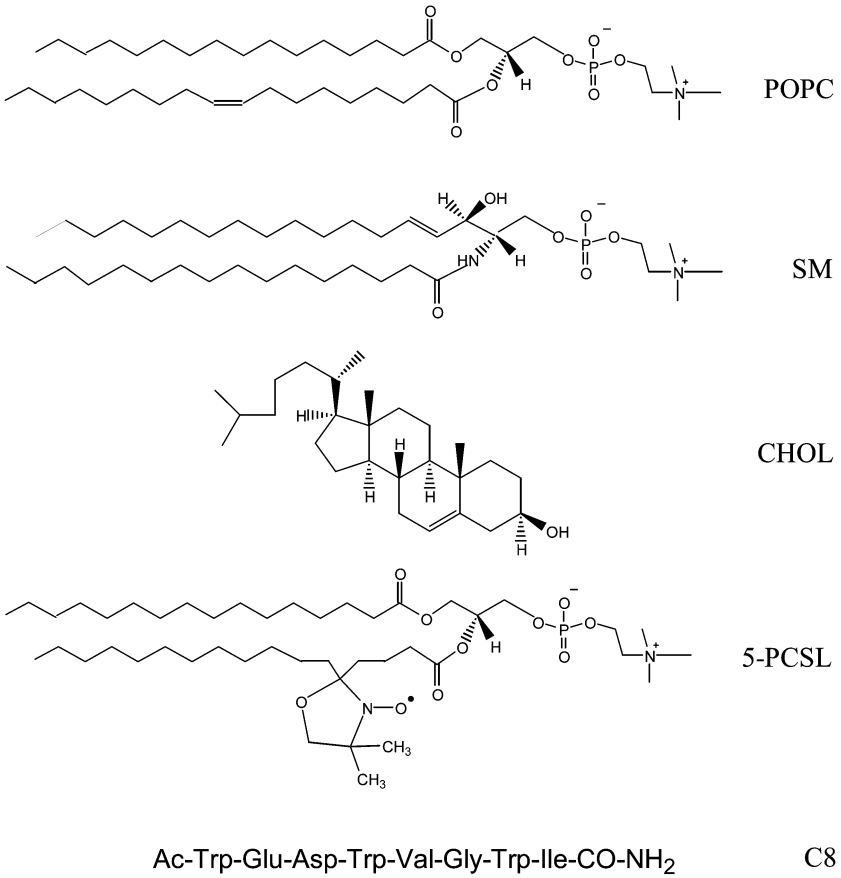

Fig. 1 Molecular formulae of POPC, SM, CHOL, 5-PCSL (chosen as an example of spin label) and amino acid sequence of the C8 peptide.

For fluorescence measurements Large Unilamellar Vesicles (LUVs) with a mean diameter of ~0.1 μm, eventually containing Rho-PE and NBD-PE in addition to unlabeled lipids, were prepared according to the extrusion method in 5 mM HEPES, 100 mM NaCl, pH 7.4, as previously described.[29] For ESR experiments, Multi-Lamellar Vesicles (MLVs), containing 1 wt % spin labeled lipids, were prepared by the lipid film method.[30] Dry lipid samples were hydrated with 20–50 μL of 10 mM phosphate buffer, 137 mM NaCl, 2.7 mM KCl, pH 7.4 (PBS), and vortexed, resulting in a MLV suspension. This suspension was transferred to a 25-μL glass capillary and flame sealed. The samples containing the peptide were prepared following the same procedure but, in this case, the lipid films were suspended with specific amounts of a C8-containing PBS solution. The peptide–lipid ratio was 0.5 : 1 wt/wt (corresponding to about 0.3 : 1 mol mol^{-1}). At this ratio the whole bilayer interacts with the peptide[17] so that only perturbed spin-labeled lipids are responsible for the ESR signal.

For neutron reflectivity experiments, Supported Lipid Bilayers (SLBs) were prepared by vesicle fusion:[31,32] Small Unilamellar Vesicles (SUVs), 25–35 nm in diameter, were formed by vortexing and sonicating for 3 × 10 min the MLV suspension. The SUV suspension (0.5 mg mL^{-1}) was injected into the NR cell, allowing diffusion and adsorption on the silicon surfaces over a period of 30 min. The solid supports for neutron reflection were 8 × 5 × 1 cm^3 silicon single crystals cut to provide a surface along the (111) plane and pre-treated as described previously.[18,31] After lipid adsorption the sample cell was rinsed once with deuterated water to remove the excess lipid. The peptide was added to the bilayer dissolved in an aqueous solution at a concentration of 0.25 mg mL^{-1} in order to obtain the 0.5 : 1 peptide/lipid weight ratio.

All measurements described below have been performed at 310 K.

2.4 Lipid mixing assays

Membrane lipid mixing was monitored using the Fluorescence Resonance Energy Transfer assay (FRET) as previously reported.[33] The assay is based on the dilution of the NBD-PE (donor) and Rho-PE (acceptor) which results in an increase in NBD-PE fluorescence. Vesicles containing 0.6 mol% of each probe were mixed with unlabeled vesicles at a 1 : 4 ratio (final lipid concentration: 0.1 mM). Small volumes of peptide in dimethylsulfoxide (DMSO) were added; the final concentration of DMSO in the peptide solution was no higher than 2% v/v. The change in donor emission was monitored as aliquots of the peptide were added to vesicles, with emission at 530 nm and excitation at 465 nm. A cut-off filter at 515 nm was used between the sample and the emission monochromator to avoid scattering interferences. The fluorescence scale was calibrated such that the zero level corresponded to the initial residual

fluorescence of the labeled vesicles and the 100% level, corresponding to complete mixing of all lipids in the system, was set by the addition of Triton X-100 (0.5% v/v) to labeled liposomes at the same total lipid concentrations of the fusion assay.[33,34] Lipid mixing experiments were repeated at least three times and results were averaged.

2.5 Inner-monolayer phospholipid-mixing (fusion) measurement

Peptide-induced phospholipid-mixing of the inner monolayer was measured by a modification of the phospholipid-mixing measurement reported elsewhere.[35] The concentration of each of the fluorescent probes within the liposome membrane was 0.6% mol/mol. LUVs with a mean diameter of 0.1 μm were prepared as described above, and subsequently treated with sodium dithionite to completely reduce the NBD-labeled phospholipid located at the outer monolayer of the membrane. The final concentration of sodium dithionite was 100 mM (from a stock solution of 1 M dithionite in 1 M TRIS, pH 10.0). The liposomal suspension was incubated for approximately 1 h on ice in the dark. Sodium dithionite was then removed by size exclusion chromatography through a Sephadex G-75 50 DNA Grade filtration column (GE Healthcare Pharmacia, Uppsala, Sweden) eluted with a buffer containing 10 mM TRIS, 100 mM NaCl, and 1 mM EDTA, pH 7.4.

2.6 Measurements of ANTS/DPX leakage

The ANTS/DPX assay was used to measure the ability of the peptide to induce leakage of ANTS/DPX pre-encapsulated in liposomes. Details of this assay can be found in the literature.[36] To initiate a leakage experiment, the peptide, in a stock solution at pH 7.4 containing 5 mM Hepes and 100 mM NaCl, was added to the stirred vesicle suspension (0.1 mM lipid).

2.7 Fluorescence titration measurements

C8–lipid bilayer interactions were also studied by monitoring the changes in the Trp fluorescence emission spectra of the peptide upon addition of increasing amounts of POPC/SM/CHOL unilamellar vesicles, as reported in previous work.[18] Fluorescence measurements were performed using a Jasco FP750 spectrofluorimeter equipped with a thermostatically controlled cuvette holder. The excitation wavelength was 280 nm and emission spectra were recorded between 310 and 450 nm, with slit widths of 2 nm. The titration was performed by adding measured amounts of a solution containing the peptide (1×10^{-4} M) and suspended lipid vesicles to a weighed amount of a solution of the peptide at the same concentration, which was initially present in the spectrofluorimetric cuvette. In this way, the lipid concentration was progressively increased (from 0 to $\sim 1 \times 10^{-3}$ M), while the peptide concentration remained constant during the whole titration. After each addition there was a 20 min wait before spectrum registration, to ensure equilibrium had been reached.

2.8 NR measurements

NR allows determination of structure and composition of layers at interfaces. Measurements were performed on the D17 reflectometer[37] at the high flux reactor of the Institut Laue-Langevin (ILL, Grenoble, France) in time-of-flight mode using a spread of wavelengths between 2 and 20 Å with two incoming angles of 0.8 and 3.2°.

The specular reflection at the silicon/water interface, R, defined as the ratio between the reflected and the incoming intensities of a neutron beam, is measured as a function of the wave vector transfer, q, perpendicular to the reflecting surface. $R(q)$ is related to the scattering length density across the interface, $\rho(z)$, which depends on the composition of the adsorbed species. The neutron scattering length density, $\rho(z)$, is defined by the following relation:

$$\rho(z) = \sum_j n_j(z) b_j \quad (1)$$

where $n_j(z)$ is the number of nuclei per unit volume and b_j is the scattering length of nucleus j.[38] The scattering lengths of the constituent fragments of any species adsorbed at the surface are the fundamental quantities from which the interfacial properties and microstructural information on the lipid bilayer are derived. Measurement of a sample in different solvent contrasts greatly enhances the sensitivity of the technique.[39]

Samples were measured using H_2O, SMW (silicon-matched water), 4MW and D_2O as solvent contrasts. SMW ($\rho = 2.07 \times 10^{-6}$ Å^{-2}) is a mixture of 38 vol% D_2O ($\rho = 6.35 \times 10^{-6}$ Å^{-2}) and 62 vol% H_2O ($\rho = -0.56 \times 10^{-6}$ Å^{-2}) with the same refraction index for neutrons as a bulk silicon, while 4MW ($\rho = 4 \times 10^{-6}$ Å^{-2}) consists of 66 vol% D_2O and 34 vol% H_2O.

Neutron reflectivity profiles were analyzed by box model fitting starting with simulations from the AFIT program.[40] The supported membrane is modelled as a series of boxes corresponding to the different bilayer regions. The program allows the simultaneous analysis of reflectivity profiles from the same sample in different water contrasts, characterizing each box by its thickness, scattering length density (ρ), solvent volume fraction, and interfacial roughness. These initial model fits were then used as templates for simultaneous fitting of the experimental data using the MOTOFIT program.[41] All the parameters were varied until the optimum fit to the data was found. Although more than one model could be found for a given experimental curve, the number of possible models was greatly reduced by a prior knowledge of the system, which allows defining upper and lower limits of the parameters to be optimized, by the elimination of the physically meaningless parameters, and most importantly by the use of different isotopic contrasts.[39] The bare silicon substrate was characterized first in terms of thickness and roughness of the native oxide layer. The set of NR profiles were calculated for a uniform single layer model (the silicon oxide layer) of thickness 8 ± 1 Å, roughness 3 ± 1 Å (8 ± 1 Å in one case), and a scattering length density of 3.41×10^{-6} Å^{-2}, corresponding to 100% SiO_2. This step was followed by the characterization of the lipid bilayer and finally of the C8-interacting bilayer.

2.9 ESR spectroscopy

ESR spectra of lipid and lipid/peptide samples were recorded on a 9 GHz Bruker Elexys E-500 spectrometer (Bruker, Rheinstetten, Germany). Capillaries containing the samples were placed in a standard 4 mm quartz sample tube containing light silicone oil for thermal stability. The temperature of the sample was maintained constant during the measurement by blowing thermostated nitrogen gas through a quartz Dewar. The instrumental settings were as follows: sweep width, 120 G; resolution, 1024 points; modulation frequency, 100 kHz; modulation amplitude, 1.0 G; time constant, 20.5 ms, incident power, 5.0 mW. Several scans, typically 32, were accumulated to improve the signal-to-noise ratio.

2.10 Molecular dynamics simulations

The starting structure for the molecular dynamics simulations of the C8 has been obtained by NMR experiments.[42] This structure was placed in a box containing a 1 : 1 : 1 POPC/SM/CHOL bilayer and water molecules in the region of the box containing only water molecules and with the Trp side chains that face towards the bilayer surface. The equilibrated bilayer was kindly provided by Pertu Niemela.[43] After the peptide insertion in the box, all water molecules with oxygen atoms closer to 0.40 nm from a non-hydrogen atom of the peptide were removed. MD simulations were performed using GROMACS 3.2 package[44] and the force field developed by Niemela *et al.*,[43] following the procedure described elsewhere.[45] In the standard GROMOS force fields a simple improper torsion with corrections for the adjacent dihedrals is used to parameterize the *cis* double bond. For the double bonds in the POPC acyl chains, we have used the description by Bachar *et al.*[46] that takes into account the skew states in the vicinity of the double bond. Independent studies have shown that this double bond description provides an important correction in both pure and cholesterol containing bilayers.[47] The Simple Point Charge (SPC) model[48] was used for water. For cholesterol, we used the description of Holtje *et al.*[49] Bond lengths were constrained using the Linear Constraint Solver (LINCS) algorithm.[50] Lennard-Jones interactions were calculated with a single 1.0 nm cutoff. Long-range electrostatic interactions were computed using the particle-mesh Ewald method[51] with a real space cut-off of 1.0 nm, spline interpolation of order 6 and direct sum tolerance of 10^{25}. Periodic boundary conditions with the usual minimum image convention were used in all three directions and the time step was set to 2 fs. The simulations were carried out in the NpT (constant particle number, pressure and temperature) ensemble at $p = 1$ atm and $T = 310$ K. Temperature and pressure were controlled by the weak coupling method[52] with the relaxation times set to 0.6 and 1.0 ps, respectively. The temperatures of the solute and solvent were controlled independently and the pressure coupling was applied separately in the bilayer plane (xy) and in the perpendicular direction (z). A total of 8 ns of equilibrated trajectory has been analyzed.

3 Results

3.1 Fusion and leakage assays

First, we investigated the effects of CHOL and SM on the ability of the C8 peptide to induce fusion between vesicles. Experiments were carried out on LUVs composed of either POPC or POPC/SM/CHOL (1 : 1 : 1). A population of vesicles labeled with both NBD- and Rho-labeled PE, used as the donor and acceptor of fluorescence energy transfer, respectively, was mixed with a population of unlabeled LUVs and increasing amounts of the peptide were added. For both lipid systems, dilution of labeled lipids *via* membrane fusion induced by the peptide resulted in a reduction of the fluorescence energy transfer efficiency, hence dequenching (increase) of the donor fluorescence and decrease of the acceptor fluorescence. In the experiment, zero percent lipid mixing was defined by the fluorescence intensity before addition of the peptide while hundred percent lipid mixing by the fluorescence intensity after the addition of Triton X-100 (0.5% v/v) to labeled liposomes at the same total lipid concentration.[34] In order to calculate the percentage of fusion, the increase of the donor fluorescence of each sample was subtracted from the blank (0% lipid mixing) and compared to its fluorescence in completely disassembled liposomes (100% lipid mixing). The dependence of the extent of lipid mixing on the peptide/lipid molar ratio was analysed (Fig. 2). The graph shows that C8 presents a higher fusogenic ability in POPC/SM/CHOL than in POPC vesicles. This is an unexpected result, the former bilayer being much more ordered and well-structured than the latter one.

In the experiments described above, the fluorescently labeled lipids equally distributed between the outer and the inner leaflets of the lipid bilayer constituting the vesicles. Consequently, they account for both hemi-fusion (fusion between the outer leaflets of two vesicles, with the inner ones delimiting two juxtaposed aqueous pools) and complete fusion (fusion of both leaflets, with complete mixing of the vesicle content). In order to discriminate between these two processes,

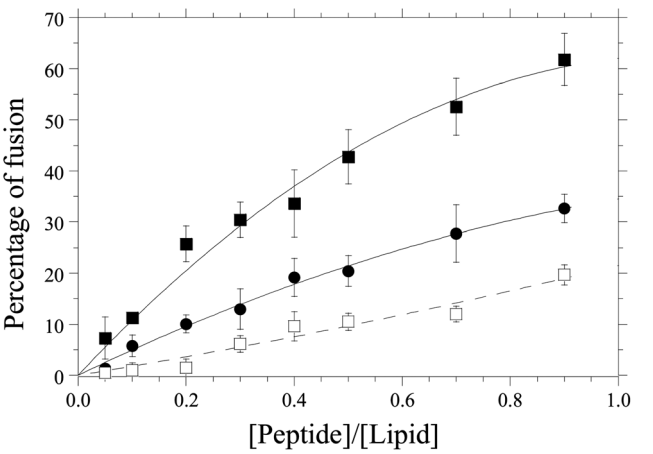

Fig. 2 C8-promoted membrane fusion of POPC (●) and POPC/SM/CHOL (1 : 1 : 1 by weight) (■) liposomes as determined by lipid mixing assays. C8-promoted fusion of the inner monolayer of POPC/SM/CHOL (□) liposomes as determined by lipid mixing assays.

we performed, for POPC/SM/CHOL vesicles, also the inner monolayer assay. In this test, the fluorescence from the outer leaflet is eliminated by the addition of an aqueous reducing agent to the liposome suspension, and the experiment reveals only the extent of lipid mixing between the inner monolayers of vesicles in solution. Fig. 2 shows a significant fusion of the inner monolayer in POPC/SM/CHOL, amounting to about 1/3 of the total fusion assay. This finding indicates that C8 is able to fuse both the inner and the outer leaflets of the lipid membranes.

Finally, in order to explore whether the interaction with the peptide facilitates molecule translocation through the lipid bilayer, we studied the C8 effect on the release of fluorophores encapsulated in POPC/SM/CHOL vesicles. A content-mixing assay was employed to monitor any mixing of internal vesicle components as a result of vesicle exposure to C8. Release of ANTS and DPX from vesicles is commonly used as a measure of bilayer perturbation and interpreted as "transient pore formation".[33,53] Our leakage experiment showed that the probe did not leak out significantly to the medium after the interaction with the peptide (data not shown). The absence of leakage indicates that, during the fusion events induced by the peptide, the bilayer integrity is preserved, so that the vesicle content is not released to the external aqueous medium.

3.2 Strength of the C8–bilayer interaction

In a first attempt to understand the increased fusogenity of C8 on POPC/SM/CHOL vesicles with respect to POPC vesicles, we verified its correlation with the tendency of the peptide to interact with the two different bilayers. Fluorescence measurements offer an opportunity to assess the strength of the C8–bilayer interaction. C8 in a buffer shows a fluorescence emission spectrum with a maximum (λ_{max}) at 356 nm, which is typical of Trp exposed to water.[54] The presence of POPC/SM/CHOL liposomes causes a slight blue shift of λ_{max} to shorter wavelength (352 nm) and a reduction of the fluorescence quantum yield (Fig. 3A). Similar results were obtained in a previous work for POPC bilayers.[18] The limited extent of the shift indicates that the bilayer-interacting Trps remain largely exposed to the solvent. Analysis of the data according to a model previously reported[18] allows estimation of the apparent peptide–lipid association constant, K_a, and the number of phospholipid molecules, n, that bind the peptide. This method requires a nonlinear best-fitting procedure of the C8 fluorescence intensities at 356 nm plotted as a function of the total lipid concentration, as shown in Fig. 3B. The K_a and n values for C8 interacting with POPC and POPC/SM/CHOL are collected in Table 1. While the average number of peptide-interacting lipids is not affected by the bilayer composition, the association constant is much larger for POPC than for POPC/SM/CHOL. Thus, it is evident that the higher peptide fusogenic activity that C8 exerts on the latter lipid system cannot be explained in terms of a stronger peptide–bilayer interaction. For this reason we undertook an investigation of the bilayer's microstructure and the effects, at a molecular level, of C8 on it. The results are reported and analyzed below.

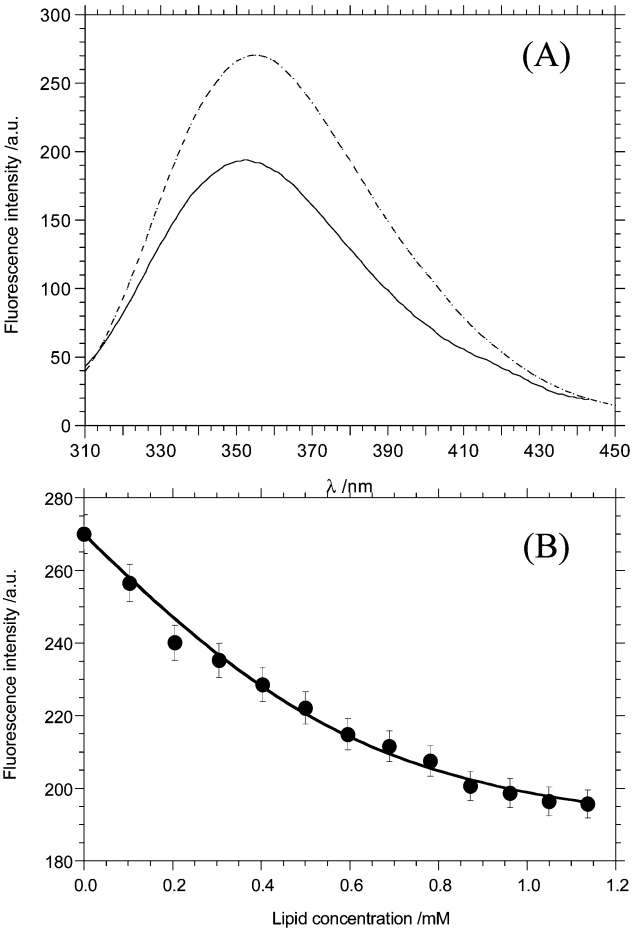

Fig. 3 C8 fluorescence reveals the peptide interaction with the POPC/SM/CHOL bilayers. (A) Emission spectra of C8 in aqueous phosphate buffer (dashed line) and in POPC/SM/CHOL unilamellar liposomes (solid line) at 1.14 mM lipid concentration. (B) Fluorescence titration curve of the C8 peptide with POPC/SM/CHOL liposomes.

Table 1 K_a (association constant between the peptide and the lipid bilayer) and n (average number of lipid molecules interacting with the peptide), estimated from C8 fluorescence titrations with POPC and POPC/SM/CHOL liposomes

	$K_a \times 10^{-3}/M^{-1}$	n
C8–POPC[a]	830 ± 60	6 ± 2
C8–(POPC/SM/CHOL)	6.6 ± 0.2	7 ± 2

[a] Data from ref. 18.

3.3 Effects of cholesterol and sphingomyelin inclusion in phospholipid bilayers

Preliminarily, POPC/SM/CHOL bilayers at 1 : 1 : 1 weight ratio were characterized by NR and ESR measurements. Bilayers formed by POPC alone have been analyzed in a previous work.[18] In order to discriminate the effects of CHOL from those of SM on the bilayer properties, lipid bilayers composed of POPC/CHOL at different weight ratios (90 : 10, 80 : 20 and 66 : 33) were also considered.

NR characterization was performed using D_2O, SMW and H_2O as isotopic contrast solvents. The experimental data and

the best fitting curves are shown in Fig. 4. The parameters used to fit the curves simultaneously from all the contrasts are given as ESI.† For all lipid systems, a five box model was found to best fit the data. The first two boxes correspond to the native oxide on the silicon block and to the thin solvent layer interposed between the silicon oxide surface and the adsorbed bilayer. The remaining three boxes describe the lipid bilayer, which is subdivided into the inner headgroups, the hydrophobic chains, and the outer headgroup layers. For all considered samples, a model without the water layer between the substrate and the bilayer gave a worse fit to the data.

The theoretical ρ values of the used lipids were calculated through eqn (1). For POPC headgroups, ρ is equal to 1.86×10^{-6} Å^{-2} while for the acyl chains it is equal to -0.29×10^{-6} Å^{-2}. For CHOL ρ is equal to 0.22×10^{-6} Å^{-2}.[55,56] In the case of SM, the calculated ρ is equal to 1.10×10^{-6} Å^{-2} for the headgroups and -0.30×10^{-6} Å^{-2} for the acyl chains. Thus, the parameters obtained from the best fit procedure are the thickness and the roughness of each box plus the solvent content expressed as volume percent. Effects of lipid composition on the thickness of each box in which the membrane can be conceptually sectioned are visualized in Fig. 5.

The presence of CHOL and SM influences the overall thickness of the lipid bilayer, which increases from 44 ± 2 Å, obtained for the pure POPC bilayers,[18] to 49 ± 2 Å obtained in the case of POPC/SM/CHOL bilayers at 1 : 1 : 1 weight ratio. In particular, the presence of cholesterol causes an increase of the thickness of the hydrophobic region, going from 28 ± 2 Å (pure POPC) to 32 ± 2 Å. At the same time, the ρ value corresponding to this region increases from -0.29 to -0.11×10^{-6} Å^{-2}. The change of the ρ value clearly confirms that cholesterol positions in the hydrophobic core between the phospholipids chains. Finally, an increase of the solvent content in the headgroup region, from ~30% in POPC to ~40% in POPC/SM/CHOL bilayers, is observed.

Interestingly, POPC/CHOL (66 : 33) bilayers roughly present the same average structural features of POPC/SM/CHOL membranes, indicating that most of these properties are determined by the presence of cholesterol in the membrane, while SM does not seem to exert any specific effect on the bilayer thickness. Perusal of Fig. 5 shows that the effect of CHOL on the bilayer thickness becomes evident above 20% by weight.

ESR investigation on the same systems was realized incorporating phosphatidylcholine spin-labeled on the different positions of the *sn*-2 chain (*n*-PCSL, with $n = 5, 7, 10, 14$) in the lipid bilayers. ESR spectra of 5-PCSL, which presents the nitroxide group close to its hydrophilic headgroup, are illustrated in Fig. 6A. All the spectra show an evident anisotropy which increases with the cholesterol content in the bilayer (continuous lines). Interestingly, the 5-PCSL spectrum in POPC/

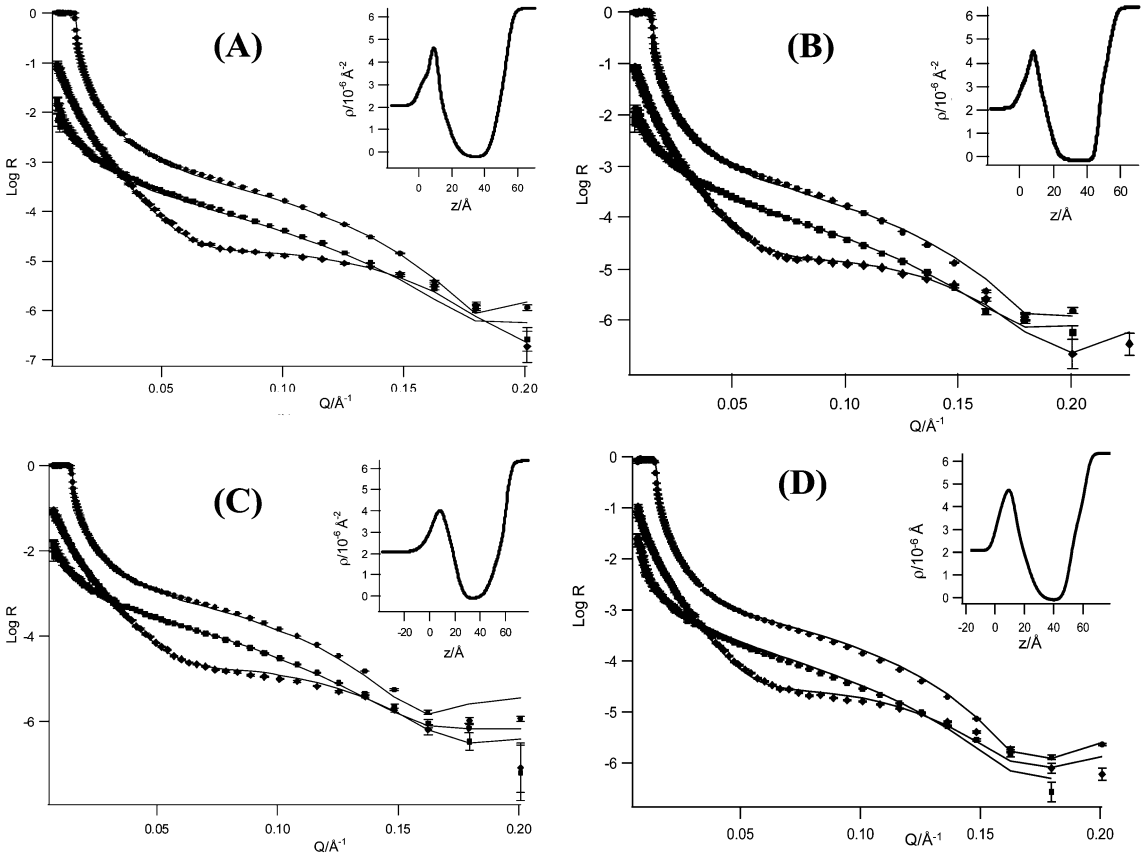

Fig. 4 Neutron reflectivity profiles (points) and best fits (continuous lines) corresponding to lipid bilayers of (A) POPC/CHOL at 90 : 10 weight ratio, (B) POPC/CHOL at 80 : 20 weight ratio, (C) POPC/CHOL at 66 : 33 weight ratio and (D) POPC/SM/CHOL at 1 : 1 : 1 weight ratio, obtained in (●) D_2O, (▲) 4MW and (◆) H_2O solvents. The insets show the ρ profile for the bilayers in D_2O.

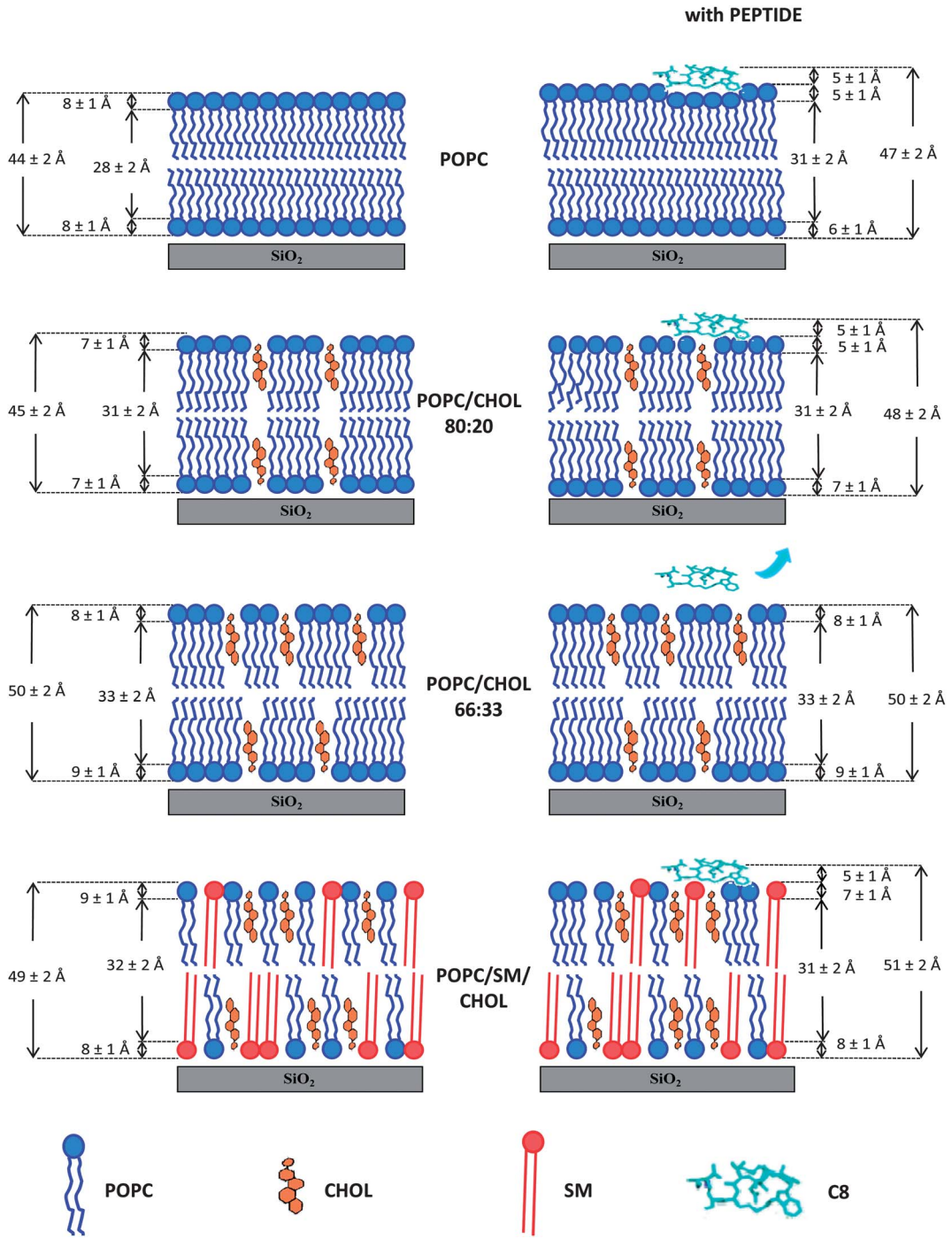

Fig. 5 Schematic representation of lipid bilayers at different lipid concentration in the absence and presence of the C8 peptide, with indication of some structural parameters obtained by NR measurements.

SM/CHOL is slightly less anisotropic than that in POPC/CHOL (66 : 33) bilayers. The same effects were observed for the ESR spectra (not shown) of 7 and 10-PCSL. We also investigated lipid bilayers including phosphatidylcholine spin labeled on the 14 C-atom of the *sn*-2 chain (14-PCSL), in which the nitroxide group is positioned close to the terminal methyl region of the chain. In this case, a narrow, three-line, quasi isotropic spectrum is obtained for POPC and POPC/CHOL 90 : 10 samples (see Fig. 6B). On further increasing the cholesterol content, a second component appears in the ESR spectra indicating that spin-labeled lipid chains have a restricted motion. In POPC/SM/CHOL bilayers, the 14-PCSL spectrum also presents the second component, even though less evident than that observed for POPC/CHOL 66 : 33 bilayers (see Fig. 6B).

A quantitative analysis of *n*-PCSL spectra for all lipid samples was realized determining the acyl chain order parameters, S, and the isotropic hyperfine coupling constants for the spin-labels in the membrane, a'_N, as described in the literature.[57] S is

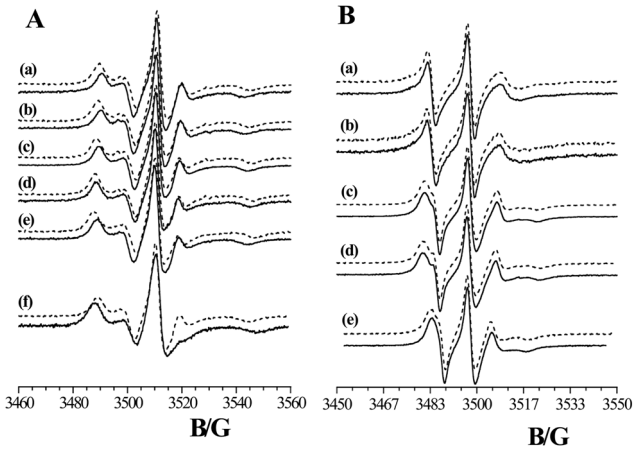

Fig. 6 ESR spectra of 5-PCSL (panel A) and 14-PCSL (panel B) in lipid bilayers of pure POPC (a), POPC/CHOL at weight ratios of 90 : 10 (b), 80 : 20 (c), 66 : 33 (d) and POPC/SM/CHOL (e) in the absence (continuous lines) and presence (dashed lines) of the C8 peptide. The ESR spectrum of 5-SMSL in a POPC/SM/CHOL bilayer (f) is also reported in panel A in the absence (continuous lines) and presence (dashed lines) of the C8 peptide.

a measure of the local orientational ordering of the labeled molecule with respect to the normal to the bilayer surface. a'_N is an index of the micropolarity experienced by the nitroxide. The values of these parameters are reported as ESI,† while Fig. 7A–7E (solid circles) show the dependence of the order parameter, *S*, on chain position, *n*, for the *n*-PCSL spin-labels in the considered bilayers. In all the investigated lipid systems, a decreasing trend is observed, as expected for bilayers in the fluid state (either L_d or L_o).[17,18,30,57–59]

To better analyze the effect of lipid composition, the *S* values for 5-PCSL and 14-PCSL are shown in Fig. 7F as a function of the CHOL content in the bilayer. For both spin-labels, *S* increases with the CHOL percentage (solid circles). In the case of 14-PCSL, the *S* increase is more marked. These results indicate that high concentrations of CHOL produce a strong effect on the lipid packing of phospholipid chains, reducing their mobility also in the terminal methyl region. In particular, perusal of Fig. 7 highlights that the external region of the bilayer is only gradually perturbed by the CHOL presence, while a sharp increase of *S* values for the inner acyl tail segments is observed between 10 and

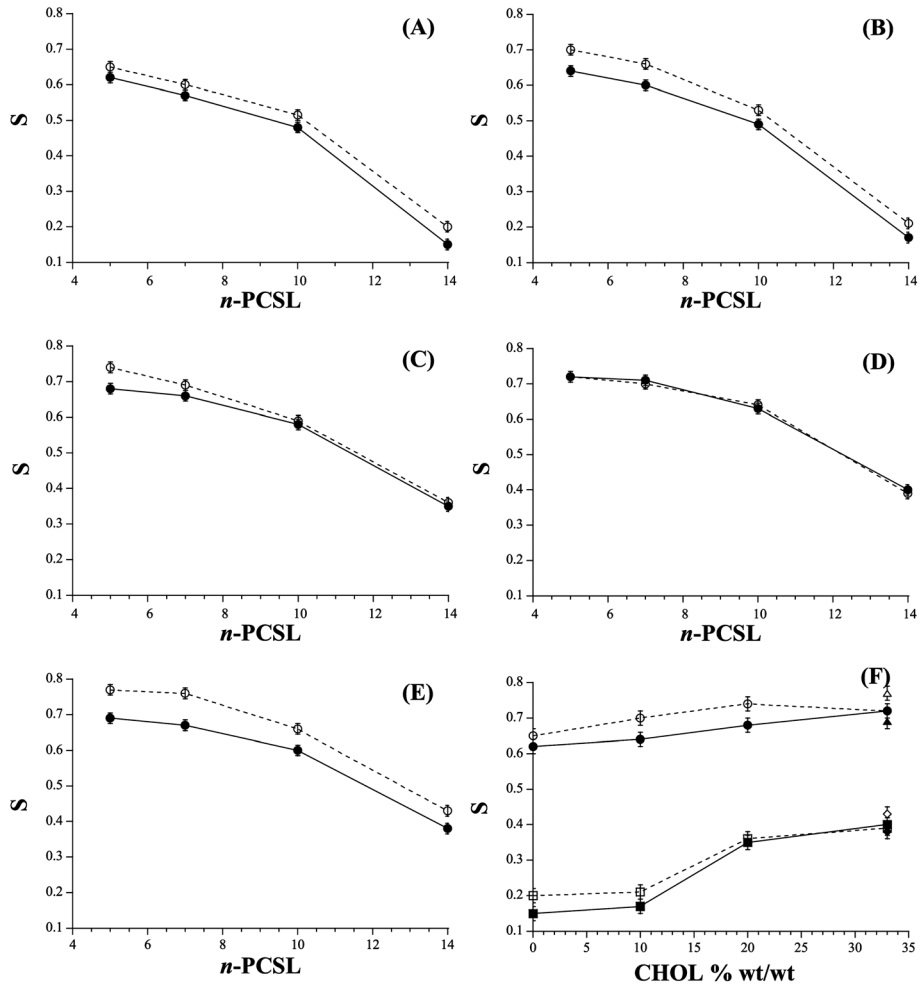

Fig. 7 Order parameter, *S*, of *n*-PCSL in a lipid bilayer of POPC (A), POPC/CHOL at 90 : 10 (B), 80 : 20 (C), 66 : 33 (D) and POPC/SM/CHOL (E) as a function of the nitroxide position, *n*, on the phospholipid acyl chains in the absence (solid circles) and presence (open circles) of the C8 peptide. In panel (F), *S* of 5-PCSL and 14-PCSL in the considered systems is reported as a function of CHOL % content, in the absence (solid symbols) and presence (open symbols) of the C8 peptide.

20% w/w of CHOL content, indicating the well-established transition of the lipid bilayer structure from a CHOL-poor fluid lamellar phase, L_d, to a CHOL-rich fluid-ordered phase, L_o.[27] It is interesting to highlight that NR shows only a gradual thickening of the hydrophobic inner core of the bilayer with increasing CHOL content. In other words, the transition is detected only by an analysis of the microscopic segmental order of lipids.

Interestingly, in the POPC/SM/CHOL bilayer the *S* values for both 5-PCSL (solid triangle) and 14-PCSL (solid diamond) are slightly lower than those obtained for POPC/CHOL (66 : 33 w/w) bilayers. For this lipid mixture, we also registered the spectrum of the sphingomyelin spin-labeled on the 5 C-atom of the *N*-acyl chain (5-SMSL). A clearly anisotropic line shape is observed, as shown in Fig. 6A (spectrum f). Interestingly, the *S* value (0.75) is remarkably higher than that derived from the 5-PCSL spectrum (0.68).

3.4 Effect of lipid composition on the interaction between the C8 peptide and lipid bilayers

The interaction of the C8 peptide with lipid membranes was initially studied by analyzing the NR curves of the fully hydrogenated lipids to which the peptide with deuterated Trp residues was added. The NR curves are shown in Fig. 8. The values of all parameters optimized in curve fitting are given as ESI.†

Similar to what was found for POPC,[18] the best fitting of the NR profiles of the POPC/SM/CHOL bilayer in the presence of the peptide requires an additional layer, as shown in Fig. 5. This layer prominently consists of the peptide interacting with the bilayer leaflet and it is characterized by a ρ value equal to 3.66×10^{-6} Å^{-2}, which corresponds to the theoretical value of the deuterated peptide calculated by eqn (1) using a molecular volume of 1410.3 Å^3.[18] Furthermore, in the presence of C8, the ρ of the external headgroup layer increases from 1.86×10^{-6} Å^{-2} to 2×10^{-6} Å^{-2}, indicating that the peptide effectively perturbs the outer hydrophilic region of the membrane. In contrast, no variations were observed in the ρ values corresponding to the hydrophobic region and the inner headgroup layer. Inspection of Fig. 5 shows that in the presence of C8 the thickness of the external headgroup layer slightly decreases. No significant changes occur in the solvent content and roughness. Furthermore, no variation of fitting parameters corresponding to the inner bilayer leaflet is observed, suggesting a membrane–peptide interaction involving only the external surface.

The C8 interaction with POPC/CHOL bilayers was also investigated by NR. In the case of POPC/CHOL 90 : 10 and POPC/CHOL 80 : 20 bilayers, a behavior similar to that observed for POPC and POPC/SM/CHOL bilayers was observed, in that an additional layer, consisting of the hydrated peptide, was necessary to obtain a good curve fitting. Also in these lipid systems, the ρ of the external headgroup region increases to $\sim 2 \times 10^{-6}$ Å^{-2} while no variation was observed in the ρ values corresponding to the hydrophobic region and inner headgroup layers. Inspection of Fig. 5 shows that for the POPC/CHOL 80 : 20 bilayer, the peptide causes a decrease of the thickness of the box modeling the external headgroup layers (by $\sim$2 Å). In contrast, no changes occurred for the chain and inner headgroup layers, indicating that also for these bilayers the peptide interaction involves only the bilayer interface.

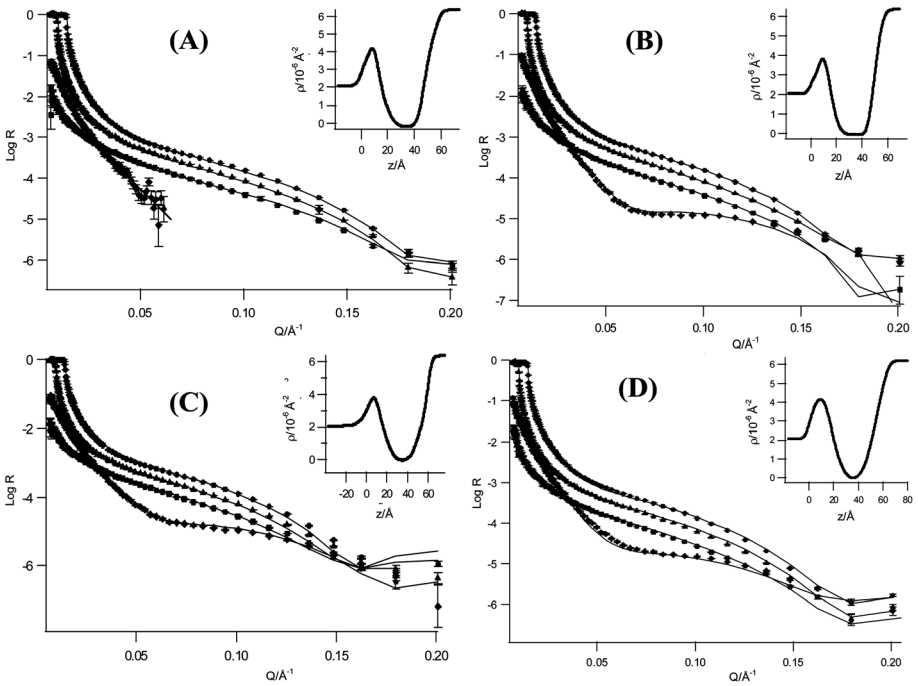

Fig. 8 Neutron reflectivity profiles (points) and best fits (continuous lines) corresponding to lipid bilayers of (A) POPC/CHOL at 90 : 10 weight ratio, (B) POPC/CHOL at 80 : 20 weight ratio, (C) POPC/CHOL at 66 : 33 weight ratio and (D) POPC/SM/CHOL at 1 : 1 : 1 weight ratio in the presence of C8-d_{5all} peptide, obtained in (●) D_2O, (▲) 4MW, (■) SMW and (◆) H_2O solvents. In the last set, data at high *Q* fall quickly into the background due to the roughness of the layer and incoherent scattering of the solvent. The insets show the ρ profile for the bilayers in D_2O.

In this scenario, the POPC/CHOL 66 : 33 bilayer is an exception. For this lipid mixture, the best fit of NR profiles in the presence of the peptide required only five model boxes and no significant change was observed in the values of all fitting parameters. This indicates that no interaction occurs between this lipid bilayer and the C8 peptide.

The C8–membrane interaction was also investigated by ESR measurements. The 5-PCSL and 14-PCSL spectra are shown in Fig. 6 (dashed lines). For POPC/SM/CHOL, POPC/CHOL 90 : 10 and POPC/CHOL 80 : 20 bilayers, the spectra show significant effects of the peptide addition, while for POPC/CHOL 66 : 33 bilayers no change was observed. A quantitative analysis of the spectra was performed by estimating the a'_N and S values. Fig. 7A–7E (open circles) show the dependence of the order parameter, S, on chain position, n, for the n-PCSL spin-labels in lipid membranes, in the presence of the C8 peptide. In the case of POPC lipid bilayers in the presence of C8, a significant increase of the S values was detected at all label positions (Fig. 7A), indicating that the ordering of the entire lipid chain is affected by the membrane–peptide interaction.

Addition of 10% w/w CHOL, which leaves the bilayer in the L_α state, does not affect the peptide–membrane interaction (Fig. 7B). The peptide also interacts with bilayers containing 20% w/w CHOL, which are in the L_o state. However, at this CHOL content, perturbation in the acyl chain order due to peptide interaction with the bilayer interface does not propagate to the inner hydrophobic core, $n \geq 7$, which remains relatively unperturbed (Fig. 7C). This finding suggests that the peptide binds solely at the membrane surface and does not penetrate appreciably into the membrane interior, as does, for instance, the HIV fusion peptide gp41-FP.[57]

For POPC/CHOL 66 : 33 bilayers no significant S change is observed at all chain positions (Fig. 7D), indicating no membrane–peptide interaction.

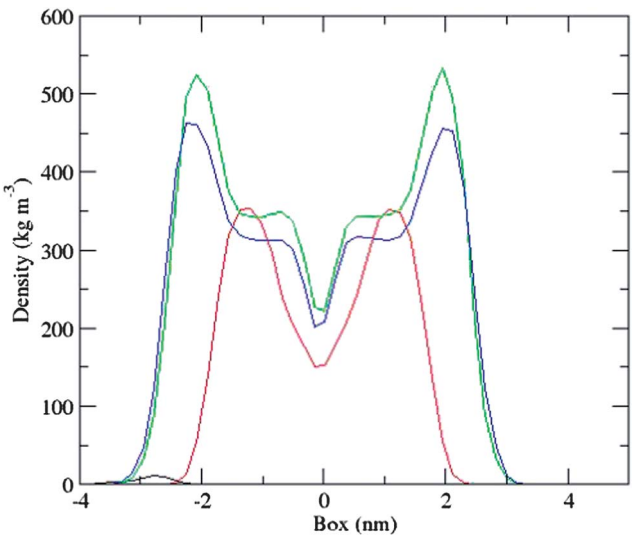

Fig. 9 Density profiles, *i.e.*, distributions, of POPC (green), SM (blue), CHOL (red), as well as C8 atoms (black) in the simulation. 0 corresponds to the center of the bilayer and the negative side corresponds to the surface region where the C8–bilayer interaction occurs.

In the case of POPC/SM/CHOL lipid bilayers, presenting the same cholesterol content of POPC/CHOL 66 : 33 bilayers, a relevant increase of S values was detected in the presence of C8 at all label positions (see Fig. 7E and the open triangle and diamond in Fig. 7F), indicating interaction of the peptide with the membrane affecting the ordering of the entire lipid chain. In the case of POPC/SM/CHOL we also investigated changes in the 5-SMSL spectrum due to the C8 peptide. Strikingly, in this case a strong reduction of the spectrum anisotropy is observed, see Fig. 6A (spectrum f), as also confirmed by the decrease of the S value (from 0.75 to 0.71).

3.5 Molecular dynamics simulations

In order to examine at atomic level the interactions between C8 and the components of the POPC/SM/CHOL bilayer, MD

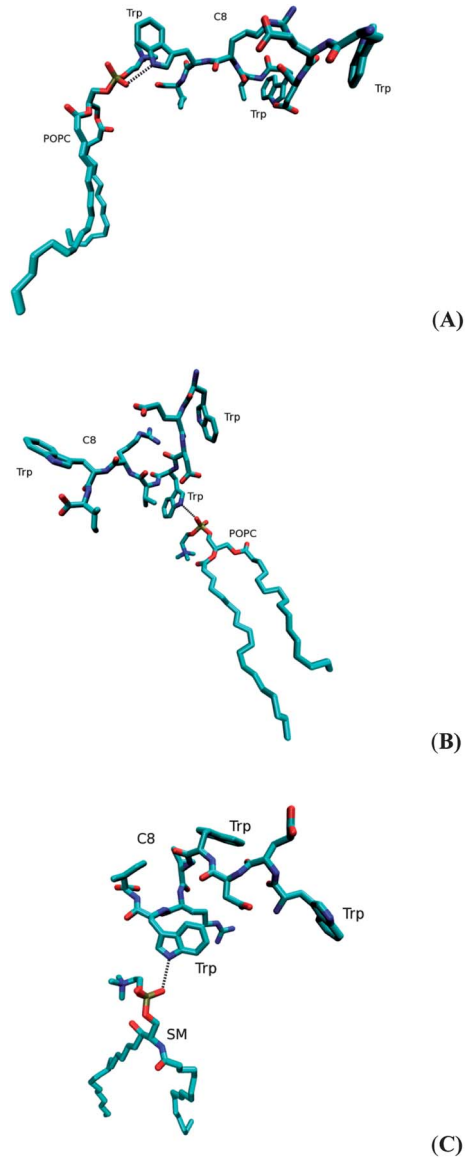

Fig. 10 Simulation snapshots showing hydrogen bonds (dashed black lines) formed between NH atoms of Trp residues and lipid molecules.

simulations were also performed. The results of the simulations were compared with those already obtained when the interactions of C8 with a POPC bilayer were studied.[18] In that study, the mass profile has been used to reveal how the different residues of C8 penetrate into the bilayer. We have shown that C8 resides on the bilayer surface and that Trp residues are critical for the positioning of the molecule in the bilayer.[18] Fig. 9 shows the mass profile for C8 in the POPC/SM/CHOL bilayer obtained by the present simulation. The projected mass density correlates well with that previously reported for C8 in the POPC bilayer, indicating that the peptide is located on the bilayer surface, in the hydrophilic region, also in the presence of SM and CHOL. A visual inspection of the trajectory and mass profile analysis of the peptide with respect to the different components of the bilayer suggests that C8 atoms are close to SM and POPC atoms, whereas they do not interact with CHOL molecules (Fig. 9).

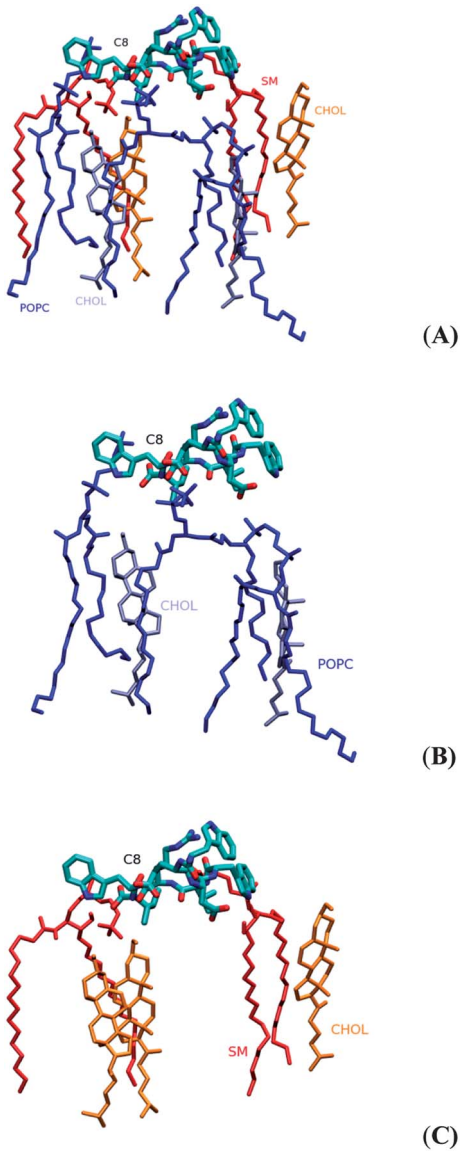

Fig. 11 (A) Simulation snapshot showing POPC (blue) and SM molecules (red) close to C8. The CHOL molecules that interact with lipids are also shown. In panels (B) and (C), CHOL interacting with POPC are colored in grey, and those in contact with SM are colored in orange.

Table 2 Number of CHOL, POPC and SM molecules interacting with the lipids that interact with C8

	POPC molecules interacting with C8	SM molecules interacting with C8
Average number of interacting CHOL molecules	0.66 ± 0.02	1.28 ± 0.02
Average number of POPC molecules	2.03 ± 0.67	2.05 ± 0.02
Average number of SM molecules	0.82 ± 0.02	0.25 ± 0.30

Fig. 10 shows snapshots of the peptide inserted in the bilayer, with the nearest lipid molecules. As can be seen, the indole NHs of Trps form direct hydrogen bonds with oxygen atom(s) of the phosphate groups of both SM and POPC. Other interesting contacts involve the CH_3 groups of the choline moiety of POPC and SM, which could form cation$\cdots\pi$ interactions with the Trp rings.

MD simulation reveals that the presence of the peptide does not provoke an increase in the solvent content at the level of the bilayer surface. This finding is in agreement with that found by NR and suggests that the enhanced fusogenic capability of C8 in the presence of CHOL and SM is not due to a change of solvent content of the bilayer, but most likely due to the interactions that the peptide can have with POPC and SM. The number of C8 neighbor molecules, where neighbors are defined as molecules that have at least one atom in close contact (<3.5 Å) with the peptide, was also evaluated. The average number of C8 neighbors in the simulation is 6–7 lipids in the POPC/SM/CHOL bilayer, whereas it has been estimated to be within 8–10 in POPC.[18] This is in very good agreement with that obtained by analyzing the fluorescence emission spectra. In particular, C8 interacts with an average of 4 POPC and 2 SM molecules, respectively. The analysis of the environments of the lipid molecules which are in direct contact with C8 reveals that they also interact with both CHOL and the other lipid (Fig. 11 and Table 2). Interestingly, the number of CHOL molecules that are close to SM molecules interacting with C8 is about two times higher than that of CHOL molecules close to peptide-interacting POPC molecules. On the other hand, C8-interacting SM molecules do not tend to be in contact with other SM molecules.

4 Discussion

In the present work, we have studied how the presence of CHOL and SM in the lipid bilayers regulates the fusogenic activity of C8, an octapeptide derived from the MPER domain of FIV gp36. The interest in this subject comes from the fact that viral envelopes are enriched in these fundamental constituents of eukaryotic cell membranes,[60] and that recent studies have

demonstrated that the effectiveness of the viral fusion depends on the lipid composition of the bilayers.[61]

Our FRET assays show that C8 fusogenic activity is much higher in POPC/SM/CHOL than in POPC. Fluorescence experiments rule out the possibility that the enhanced C8 functionality is caused by a stronger binding of the peptide to POPC/SM/CHOL bilayers, the apparent peptide–lipid association constant, K_a, being much higher for POPC bilayers than for mixed membranes. Fluorescence results also show that C8 binds at the bilayer interface, interacting with a relatively low number of lipids (~6), independent of the bilayer lipid composition.

At this point, we recognized that in order to clarify the reasons for the enhanced C8 fusogenic activity in the presence of CHOL and SM, the peptide–lipid interaction was to be analyzed in much deeper molecular detail. This was achieved by ESR and NR experiments, along with MD simulations.

Before going on with the discussion of the experimental and computational results, it is worthwhile to briefly summarize here the molecular features of the considered lipids. POPC and SM share the same zwitterionic headgroup, while the hydrophobic parts of their molecules are significantly different (Fig. 1). Because of the presence of the amide bond and the free hydroxyl, SM carries both H-bond acceptor and donor properties. In contrast, POPC can only act as a H-bond acceptor.[62] Furthermore, the presence of a *cis* double bond in the middle of one of the POPC acyl chains hinders a tight and ordered packing of neighbouring lipid tails, while SM chains are much more prone to align along the lipid bilayer normal.

A CHOL molecule presents only one hydroxyl as the hydrophilic moiety while its hydrophobic portion is relatively bulkier. Consequently, in order to be shielded from the contact with water, CHOL requires that the headgroups of the neighbouring lipids in the bilayer bend on it, according to the so-called "umbrella model".[63] Furthermore, its hydrophobic portion is mostly constituted by a semi-rigid tetracyclic ring system. From a microscopic viewpoint, its insertion among the acyl chains of the other lipids increases their order and rigidity.[64] In the preliminary study conducted on lipid samples in the absence of a peptide, we have found that addition of CHOL to POPC induces a lipid bilayer transition from a liquid-disordered (L_d or L_α) to a liquid ordered (L_o) state. On the other hand, at the composition used in this study (1 : 1 : 1 weight ratio), the entire POPC/SM/CHOL bilayer is in the L_o state,[27] with no segregation of lipids to form mesoscopic domains.

The comparison between POPC/CHOL at 66 : 33 w/w and POPC/SM/CHOL (1 : 1 : 1) bilayers is particularly interesting, since they contain the same CHOL amount and consequently allow a direct analysis of the SM effect on the bilayer properties. NR data indicate that, on the average, these two bilayers present similar thickness and mesostructure. Interestingly, ESR data show SM chains to be more ordered than POPC ones. This suggests a preference of CHOL to locate close to SM. Indeed, the presence of a single mesoscopic lipid arrangement does not mean that the microscopic distribution of the three components within the bilayer is purely statistical. Preferential interactions between SM and CHOL molecules are related to the higher SM ability to form H-bond with the CHOL hydroxyls,[65] in combination with hydrophobic and van der Waals interactions between the molecules.[66–68] In contrast, the interactions between CHOL and POPC have been proposed to be much weaker due to the disturbing effect of the *cis* double bond in the *sn*-2 chain of POPC molecules on the packing between phospholipids and sterol in the monolayer.[69] As a consequence, a microscopically inhomogeneous lipid distribution could occur in POPC/SM/CHOL, with SM and CHOL forming transient, dynamic, and unstable associations leaving the POPC relatively "free".[70]

Our results clearly show that lipid composition modulates the interaction of the bilayer with the C8 peptide. C8 interacts with POPC bilayers, as discussed by us in a previous work.[18] The presence of low CHOL amounts does not affect the peptide–membrane interaction, as highlighted by both NR and ESR data. In contrast, the peptide does not interact at all with POPC bilayers containing CHOL at 33% w/w. This evidence suggests that CHOL indirectly modulates the C8–membrane interaction by inducing more ordered and tightly packed spatial arrangement of the phospholipids. Consequently the phosphocholine groups forming the membrane interface lose the ability to dynamically re-arrange in order to accommodate the approaching peptide. Indeed, the lipid's aptitude to re-organize the local curvature and even to form non-lamellar structures has been proposed to be fundamental in modulating peptide–membrane interactions.[71,72] In connection to this, it is worth mentioning that recent studies have identified a membrane curvature selective mode of interaction of other peptides derived from viral fusion proteins.[73–75]

Both NR and ESR data show that POPC/SM/CHOL (1 : 1 : 1) bilayers interact with the C8 peptide. Similar to that observed in POPC bilayers, the peptide locates at the membrane interface, affecting the lipid's order and dynamics. ESR data specifically indicate that the peptide effect propagates along the POPC acyl chain until the deep interior of the bilayer, inducing a significant reduction of the segmental acyl chain mobility. Our MD simulations allow an investigation of the reason why the presence of SM favours the peptide–membrane interaction. First, simulations rule out that the peptide positioning at the membrane interface could be driven by selective C8–SM interactions. Indeed, molecular interactions between C8 and the lipids involve the Trps and the lipid headgroups, which are the same for SM and POPC. Specific SM groups (the free hydroxyl and the amide group) are not involved in the interaction with the peptide. Moreover, the number of POPC headgroups in contact with each C8 molecule is nearly double than that of SM headgroups. Thus, it seems that POPC drives the membrane interaction with C8 in POPC/SM/CHOL (1 : 1 : 1) bilayers while in POPC/CHOL (66 : 33 w/w) bilayers it completely loses this capability. This different behaviour could be connected with the inhomogeneous lipid distribution in the bilayer, which generates the local microscopic structure needed to establish the interaction with the peptide. Because of the CHOL preference to interact with SM, POPC enriched regions transiently form, in which the lipid headgroups maintain their ability to interact with the peptide, driving its positioning at the membrane

interface. Here, C8 comes in contact also with CHOL-interacting SM molecules, causing strong perturbations in the order parameter of their hydrophobic tails, as highlighted by ESR results. Particularly, the outer segments of the C8-interacting SM tails ($n = 5$) assume a much less ordered conformation, which necessarily reflects in a destabilization of the membrane microdomains rich in SM and CHOL. This effect could justify the higher C8 fusogenic activity on POPC/SM/CHOL membranes with respect to POPC ones. It is worth highlighting that in biphasic lipid mixtures the tendency of C8 to locate at the boundary between POPC-rich and SM-rich regions of the membrane could affect the line tension between lipid domains. In turn, line tension plays a critical role in determining dimension, shape and number of domains.[76–78] Thus, our results support the idea that not only transmembrane peptides affect lipid domain formation,[79–81] but also peptides interacting with the bilayer interface.

Our results suggest a strict interplay among the different lipids in the peptide-induced fusion mechanism. Despite CHOL not directly coming in contact with C8, its inhomogeneous distribution within the bilayer appears to be of fundamental relevance: the peptide interacting with relatively CHOL-enriched SM molecules causes a strong perturbation of the local lipid order, which is a necessary condition for membrane fusion.

Finally, our experimental results shed a new light on the lipid involvement in biological membrane processes. Effects of single lipids (*e.g.*, sphingolipids or sterols) are not to be necessarily connected to their direct participation in the process or to a totally aspecific change in membrane properties (*e.g.*, fluidity and permeability), but rather to the indirect perturbation of the specific interlipid interactions.

Acknowledgements

The authors thank MIUR (PRIN 2010-2011, grant number 2010NRREPL) for financial support and the Institut Laue-Langevin for awarding beam time and providing support to GV, during his internship placement as a visitor scientist, within the PSCM initiative.

References

1 B. Davletov and C. C. Montecucco, *Curr. Opin. Neurobiol.*, 2010, **20**, 543.
2 L. J. Pike, *J. Lipid Res.*, 2009, **50**(suppl.), S323.
3 C. Dart, *J. Physiol.*, 2010, **588**(Pt 17), 3169.
4 C. L. Schengrund, *Brain Res. Bull.*, 2010, **82**, 7.
5 W. Dowhan, *J. Lipid Res.*, 2009, **50**(suppl.), S305.
6 M. A. De Matteis and A. Godi, *Biochim. Biophys. Acta*, 2004, **1666**, 264.
7 W. Dowhan and M. Bogdanov, *Biochim. Biophys. Acta*, 2012, **1818**, 1097–1107.
8 S. E. Blondelle, K. Lohner and M. I. Aguilar, *Biochim. Biophys. Acta*, 1999, **1462**, 89.
9 J. Fantini and N. Yahi, *Expert Rev. Mol. Med.*, 2010, **12**, e27.
10 T. Balla, *J. Cell Sci.*, 2005, **118**, 2093.
11 G. R. Guzman, A. Ortiz-Acevedo, J. Santiago, L. V. Rojas and J. A. Lasalde-Dominicci, *Recent Res. Dev. Membr. Biol.*, 2002, **1**, 127.
12 E. Posse de Chaves, *Can. J. Physiol. Pharmacol.*, 2012, **90**, 753.
13 G. Vitiello, M. Grimaldi, A. M. D'Ursi and G. D'Errico, *Biochem. Biophys. Res. Commun.*, 2012, **417**, 88.
14 B. Brugger, B. Glass, P. Haberkant, I. Leibrecht, F. T. Wieland and H. G. Krausslich, *Proc. Natl. Acad. Sci. U. S. A.*, 2006, **103**, 2641.
15 S. C. Harrison, *Nat. Struct. Mol. Biol.*, 2008, **15**, 690.
16 M. Lorizate, N. Huarte, A. Saez-Cirion and J. L. Nieva, *Biochim. Biophys. Acta*, 2008, **1778**, 1624.
17 G. D'Errico, G. Vitiello, A. M. D'Ursi and D. Marsh, *Eur. Biophys. J.*, 2009, **38**, 873.
18 A. Merlino, G. Vitiello, M. Grimaldi, F. Sica, E. Busi, R. Basosi, A. M. D'Ursi, G. Fragneto, L. Paduano and G. D'Errico, *J. Phys. Chem. B*, 2012, **116**, 401.
19 H. Aizaki, K. Morikawa, M. Fukasawa, H. Hara, Y. Inoue, H. Tani, K. Saito, M. Nishijima, K. Hanada, Y. Matsuura, M. M. Lai, T. Miyamura, T. Wakita and T. Suzuki, *J. Virol.*, 2008, **82**, 5715.
20 V. I. Razinkov and F. S. Cohen, *Biochemistry*, 2000, **39**, 13462.
21 T. W. Mitchell, K. Ekroos, S. J. Blanksby, A. J. Hulbert and P. L. Else, *J. Exp. Biol.*, 2007, **210**, 3440.
22 D. Marsh and A. Watts, in *Lipid-Protein Interactions*, ed. P. C. Jost and O. H. Griffith, Wiley Interscience, New York, 1982, vol. 2, p. 53.
23 D. Marsh, *Curr. Opin. Colloid Interface Sci.*, 1997, **2**, 4.
24 M. I. Collado, F. M. Goñi, A. Alonso and D. Marsh, *Biochemistry*, 2005, **44**, 4911.
25 D. Marsh, *Biochim. Biophys. Acta*, 2009, **1788**, 2114.
26 R. F. M. de Almeida, A. Fedorov and M. Prieto, *Biophys. J.*, 2003, **85**, 2406.
27 D. Marsh, *Biochim. Biophys. Acta*, 2010, **1798**, 688.
28 C. R. Mateo, A. U. Acuna and J.-C. Brochont, *Biophys. J.*, 1995, **68**, 978.
29 R. Tarallo, A. Accardo, A. Falanga, D. Guarnieri, G. Vitiello, P. Netti, G. D'Errico, G. Morelli and S. Galdiero, *Chem.–Eur. J.*, 2011, **17**, 12659.
30 A. Falanga, R. Tarallo, G. Vitiello, M. Vitiello, E. Perillo, M. Cantisani, G. D'Errico, M. Galdiero and S. Galdiero, *PLoS One*, 2012, **7**, e32186.
31 B. W. Koenig, S. Kruger, W. J. Orts, C. F. Majkrzak, N. F. Berk, J. V. Silverton and K. Gawrisch, *Langmuir*, 1996, **12**, 1343.
32 H. P. Wacklin and R. K. Thomas, *Langmuir*, 2007, **23**, 7644.
33 S. Galdiero, A. Falanga, M. Vitiello, H. Browne, C. Pedone and M. Galdiero, *J. Biol. Chem.*, 2005, **280**, 28632.
34 S. Shnaper, K. Sackett, S. A. Gallo, R. Blumenthal and Y. Shai, *J. Biol. Chem.*, 2004, **279**, 18526.
35 A. Falanga, M. T. Vitiello, M. Cantisani, R. Tarallo, D. Guarnieri, E. Mignogna, P. Netti, C. Pedone, M. Galdiero and S. Galdiero, *Nanomedicine*, 2011, **7**, 925.
36 H. Ellens, J. Bentz and F. C. Szoka, *Biochemistry*, 1984, **23**, 1532.
37 R. Cubitt and G. Fragneto, *Appl. Phys. A: Mater. Sci. Process.*, 2004, **74**(suppl.), S329.
38 J. S. Higgins and H. C. Benoitt, *Polymers and Neutron Scattering*, Clarendon Press, Oxford, 1994.

39 G. Fragneto, R. K. Thomas, A. R. Rennie and J. Penfold, *Langmuir*, 1996, **12**, 6036.
40 P. N. Thirtle, *Afit simulation program, v. 3.1*, 1997.
41 A. Nelson, *J. Appl. Crystallogr.*, 2006, **39**, 273.
42 S. Giannecchini, A. Di Fenza, A. M. D'Ursi, D. Matteucci, P. Rovero and M. Bendinelli, *J. Virol.*, 2003, **77**, 3724.
43 P. S. Niemela, S. Ollila, M. T. Hyvonen, M. Karttunen and I. Vattulainen, *PLoS Comput. Biol.*, 2007, **3**, e34.
44 E. Lindahl, B. Hess and D. van der Spoel, *J. Mol. Model.*, 2001, **7**, 306.
45 P. S. Niemela, M. T. Hyvonen and I. Vattulainen, *Biochim. Biophys. Acta*, 2009, **1788**, 122.
46 M. Bachar, P. D. Brunelle, P. Tieleman and A. Rauk, *J. Phys. Chem. B*, 2004, **108**, 7170.
47 H. Martinez-Seara, T. Tomasz Róg, M. Karttunen, R. Reigada and I. Vattulainen, *J. Chem. Phys.*, 2008, **129**, 105103.
48 H. J. C. Berendsen, J. P. M. Postma, W. F. van Gunsteren and J. Hermans, in *Intermolecular Forces*, ed. B. Pullman, Reidel, Dordrecht, The Netherlands, 1981.
49 M. Holtje, T. Forster, B. Brandt, T. Engels, W. von Rybinski and H. D. Höltje, *Biochim. Biophys. Acta*, 2001, **1511**, 156.
50 B. Hess, H. Bekker, H. J. C. Berendsen and J. G. E. M. Fraaije, *J. Comput. Chem.*, 1997, **18**, 1463.
51 D. M. York, T. A. Darden and L. G. Pedersen, *J. Chem. Phys.*, 1993, **99**, 8345.
52 H. J. C. Berendsen, J. P. M. Postma, W. F. van Gunsteren, A. Di Nola and J. R. Haak, *J. Chem. Phys.*, 1984, **81**, 3684.
53 R. A. Parente, S. Nir and F. C. Szoka Jr, *Biochemistry*, 1990, **29**, 8713.
54 L. Ambrosone, G. D'Errico and R. Ragone, *Spectrochim. Acta*, 1997, **53**, 1615.
55 H. P. Vacklin, F. Tiberg, G. Fragneto and R. K. Thomas, *Biochemistry*, 2005, **44**, 2811.
56 B. Deme and L. Lang-Theng, *J. Phys. Chem. B*, 1997, **101**, 8250.
57 S. Galdiero, A. Falanga, G. Vitiello, M. Vitiello, C. Pedone, G. D'Errico and M. Galdiero, *Biochim. Biophys. Acta*, 2010, **1798**, 579.
58 R. Spadaccini, G. D'Errico, V. D'Alessio, E. Notomista, A. Bianchi, M. Merola and D. Picone, *Biochim. Biophys. Acta*, 2010, **1798**, 344.
59 G. Mangiapia, G. D'Errico, L. Simeone, C. Irace, A. Radulescu, A. Di Pascale, A. Colonna, D. Montesarchio and L. Paduano, *Biomaterials*, 2012, **33**, 3770.
60 L. Kalvodova, J. L. Sampaio, S. Cordo, C. S. Ejsing, A. Shevchenko and K. Simons, *J. Virol.*, 2009, **83**, 7996.
61 G. Vitiello, A. Falanga, M. Galdiero, D. Marsh, S. Galdiero and G. D'Errico, *Biochim. Biophys. Acta*, 2011, **1808**, 2517.
62 B. Ramstedt and J. P. Slotte, *Biochim. Biophys. Acta*, 2006, **1758**, 1902.
63 J. Huang, J. T. Buboltz and G. W. Feigenson, *Biochim. Biophys. Acta*, 1999, **1417**, 89.
64 H. Martinez-Seara, T. Rog, M. Karttunen, I. Vattulainen and R. Reigada, *PLoS One*, 2010, **5**, e11162.
65 J. Zidar, F. Merzel, M. Hodošček, K. Rebolj, K. Sepčić, P. Maček and D. Janežič, *J. Phys. Chem. B*, 2009, **113**, 15795.
66 P. Wydro, M. Flasiński and M. Broniatowski, *J. Colloid Interface Sci.*, 2013, **397**, 122.
67 M. Lönnfors, J. P. F. Doux, J. A. Killian, T. K. M. Nyholm and J. P. Slotte, *Biophys. J.*, 2011, **100**, 2633.
68 E. J. Aittoniemi, P. S. Niemelä, M. T. Hyvönen, M. Karttunen and I. Vattulainen, *Biophys. J.*, 2007, **92**, 1125.
69 P. Wydro, S. Knapczyk and M. Łapczyńska, *Langmuir*, 2011, **27**, 5433.
70 A. Bunge, P. Müller, M. Stöckl, A. Herrmann and D. Huster, *Biophys. J.*, 2009, **94**, 2680.
71 R. M. Epand, *Biochim. Biophys. Acta*, 1998, **1379**, 353.
72 E. Strandberg, J. Zerweck, P. Wadhwani and A. S. Ulrich, *Biophys. J.*, 2013, **104**, L09.
73 N. J. Cho, H. Dvory-Sobol, A. Xiong, S. J. Cho, C. W. Frank and J. S. Glenn, *ACS Chem. Biol.*, 2009, **4**, 1061.
74 G. J. Hardy, R. Nayak, S. Munir Alam, J. G. Shapter, F. Heinrich and S. Zauscher, *J. Mater. Chem.*, 2012, **22**, 19506.
75 B. Barz, T. C. Wong and I. Kosztin, *Biochim. Biophys. Acta*, 2008, **1778**, 945.
76 F. A. Heberle, R. S. Petruzielo, J. Pan, P. Drazba, N. Kučerka, R. F. Standaert, G. W. Feigenson and J. Katsaras, *J. Am. Chem. Soc.*, 2013, **135**, 6853.
77 M. B. Sankaram, D. Marsh, L. M. Gierasch and T. E. Thompson, *Biophys. J.*, 1994, **66**, 1959.
78 J. E. Shaw, R. F. Epand, J. C. Y. Hsu, G. C. H. Mo, R. M. Epand and C. M. Yip, *J. Struct. Biol.*, 2008, **162**, 121.
79 J. Domański, S. J. Marrink and L. V. Schäfer, *Biochim. Biophys. Acta*, 2012, **1818**, 984.
80 P. Pathak and E. London, *Biophys. J.*, 2011, **101**, 2417.
81 J. A. Poveda, A. M. Fernández, J. A. Encinar and J. M. González-Ros, *Biochim. Biophys. Acta*, 2008, **1778**, 1583.